# Achieving Reproducible Performance of Electrochemical, Folding Aptamer-Based Sensors on Microelectrodes: Challenges and Prospects

Juan Liu, Samiullah Wagan,[†] Melissa Dávila Morris,[‡] James Taylor,[§] and Ryan J. White*

Department of Chemistry and Biochemistry, University of Maryland Baltimore County, 1000 Hilltop Circle, Baltimore, Maryland 21250, United States

S *Supporting Information*

ABSTRACT: Combining specific recognition capabilities with the excellent spatiotemporal resolution of small electrodes represents a promising methodology in bioanalytical and chemical sensing. In this paper, we report the development of reproducible electrochemical, aptamer-based (E-AB) sensors on a gold microelectrode platform. Specifically, we develop microscale sensors (25 μm diameter) for two representative small molecule targets—adenosine triphosphate and tobramycin. Furthermore, we report on the challenges encountered at this size scale including small-magnitude signals and interference from the irreversible reduction of dissolved oxygen and present methods to circumvent these challenges. Through the electrochemical deposition of dendritic gold nanostructures, we demonstrate microscale sensors with improved performance by increasing signal-to-noise and consequently sensitivity. Finally, we report on the use of the nonspecific adsorption of serum proteins as an additional layer of surface passivation for stable sensor performance. The sensor development here represents general guidelines for fabricating electrochemical, folding aptamer-based sensors on small-scale electrodes.
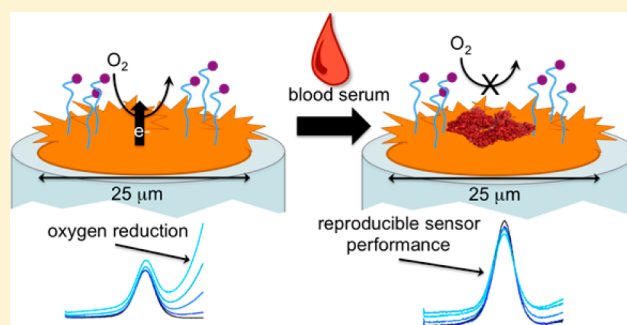
Electrochemical methods have attracted tremendous focus and efforts as a core analytical tool in the design of chemical and biological sensors.[1−6] This focus is a result of the combined selectivity and sensitivity that electrochemical interrogation affords. The development of micro- and nano-electrodes has further pushed electrochemical sensing into new space and time domains. Small-scale electrodes, with a critical dimension approaching that of the diffuse layer (radius of <~25 μm)[7] offer advantages such as fast mass transfer, small RC time constants, and low ohmic drops all of which provide exceptional spatiotemporal resolution over macroscale electrodes.[7,8] With these improvements, small-scale electrodes have found utility in scanned probe techniques, such as scanning electrochemical microscopy (SECM),[9−12] single-cell measurements,[13−15] and in vivo measurements.[16−18] To add further functionality, electrode surface modification can add specific analyte recognition. As such, microelectrodes and nano-electrodes have been modified with enzymes[19−21] and nucleic acids[22−26] for the development of sensitive biosensors.

Relying on the promising attributes of electrochemical detection schemes, aptamer-based recognition has become a popular method to impart chemical specificity into chemical and biochemical sensors. Aptamers are short DNA or RNA sequences selected in vitro to bind a specific target.[27,28] Coupled with electrochemical detection, electrochemical, aptamer-based (E-AB) sensors represent a class of sensors that is reagentless, reusable, rapid, sensitive, and specific.[29−32]

This class of sensor typically relies on a redox-labeled, electrode-bound sensing aptamer to undergo a conformation and/or flexibility change (i.e., fold) in the presence of target analyte (Scheme 1).[33] The folding of the aptamer alters the electron transfer efficiency between the distal-attached redox

Scheme 1. Electrochemical Aptamer-Based Sensors Utilize a Target-Induced Conformation Change in the Aptamer to Generate Analyte Specific Changes in Signal[a]
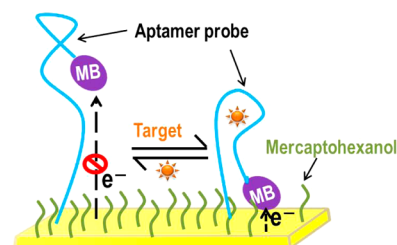
[a]The target-induced conformation change alters the efficiency with which a covalently attached redox molecule (MB) can exchange electrons with the electrode surface. This change in efficiency is readily measured using voltammetric methods.

probe and electrode surface and as such sensor signaling is readily measured voltammetrically.[34] There are many reports of this class of sensor on large-scale electrodes (2 mm diameter),[30,31,35−40] however to the best of the authors' knowledge, reproducible and quantitative folding-based sensors on microelectrodes (critical dimension of <~25 μm) have not been reported.

In this Article, we combine the spatiotemporal resolution of microelectrodes and the chemical specificity of folding aptamer-based recognition to create sensors with improved sensitivities over macroscale sensors. Specifically, we report for the first time the use of 25-μm-diameter gold electrodes as a platform for the fabrication of reproducible E-AB sensors for two representative targets: adenosine triphosphate (ATP) and the aminoglycoside antibiotic tobramycin. To circumvent small sensor currents and large background currents, we electrodeposit dendritic gold nanostructures to increase electrode surface area while maintaining the microelectrode geometric footprint. We find that the use of a nanostructured surface improves sensor performance in terms of signal-to-noise and stability. Furthermore, we observe that employing the microsensors in 100% undiluted fetal bovine serum decreases background currents from the reduction of dissolved oxygen thus allowing for improved sensor performance and demonstrate that the nonspecific adsorption on serum proteins act to further passivate the electrode surface area. As this is a work in progress, we highlight the challenges and prospects of electrochemical, aptamer-based sensors built on small-scale electrodes. The protocols presented here represent general guidelines for the development of electrochemical sensors with unprecedented spatiotemporal resolution and chemical specificity.

MATERIALS AND METHODS

Materials and Chemicals. Unless otherwise noted, all chemicals and materials were used as received. 25-μm-diameter gold wire (99.95%) and silver conductive adhesive paste were obtained from Alfa Aesar. For microelectrode fabrication, soda lime glass capillaries (LB16, 1.65 mm outer diameter, 1.10 mm inner diameter) and tungsten rods (0.010 × 3 in.) were acquired from Dagan Corporation (Minneapolis, MN) and A-M Systems, Inc. (Sequim, WA) respectively. Microcut discs (240 grit, 600 grit and 1200 grit), microcloth, 1 μm monocrystalline diamond solution, and 0.05 μm alumina micropolish for polishing electrodes were purchased from Buehler (Lake Bluff, Il). Gold(III) chloride trihydrate, hydrochloric acid (37%), sodium chloride, Trizma base (2-amino-2-(hydroxymethyl)-1, 3-propanediol), magnesium chloride, tris-2-carboxyethyl-phosphine hydrochloride (TCEP), 6-mercapto-1-hexanol (99%), tobramycin sulfate salt, and fetal bovine serum were all used as receive from Sigma-Aldrich without further purification. Solutions were prepared using ultrapure water (Mili-Q Ultrapure Water Purification, Milipore, Billerica, MA). Tris buffer contained 100 mM sodium chloride, 20 mM Trizma base and 5 mM magnesium chloride. Gold(III) electrodepositing solution includes 1.2 mg/mL gold chloride, 1.5 wt % hydrochloric acid and 0.1 M sodium chloride. Previously reported DNA aptamer probe sequences (see below) were synthesized and purified using dual-HPLC (Biosearch Technologies, Inc., Novato, CA).[35,38,41,42] The aptamers were stored at 200 μM in autoclaved 0.01 M EDTA aqueous solution (pH 8.0, Sigma-Aldrich) at −20 °C until use. The aptamer sequences adapted from the literature were modified at the

5′-end with a six-carbon-thiol (HSC$_6$) and at the 3′-terminus with the redox active methylene blue (MB). Of note, the original tobramycin aptamer reported in the literature is a RNA aptamer for aminoglycoside antibiotics. The sequence used in this study is a DNA sequence previously developed and demonstrated to specifically bind aminoglycoside antibiotics by Rowe at al.[35] ATP aptamer sequence:[38] 5′-HSC$_6$-CTGGGG-GAGTATTGCGGAGGAAA-MB-3′. Tobramycin aptamer sequence:[35] 5′-HSC$_6$-GGGACTTGGTTTAGGTAATGAGTC-CC-MB-3′.

Microelectrode Fabrication. Gold microelectrode fabrication was carried out using well-established methods.[8,43−45] Briefly, a 25 μm-diameter gold wire was attached to a tungsten rod using conductive silver epoxy. The gold−tungsten assembly was then inserted into a soda lime glass capillary and then the gold wire was sealed into the capillary using a natural gas-oxygen flame. The other end of the assembly was secured with a resin epoxy. Finally, the excess insulating glass is removed through manual polishing on sand paper (from rough to fine grit) to expose a gold wire resulting in a microdisk electrode with a 25 μm diameter.
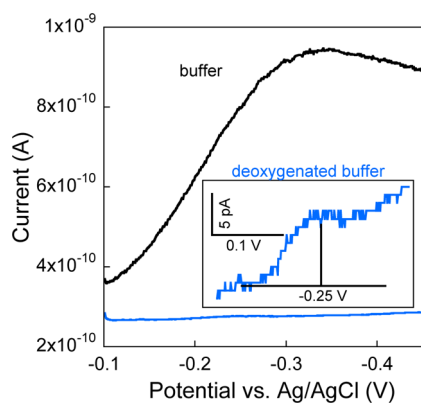
Sensor Fabrication and Interrogation. Electrochemical, aptamer-based (E-AB) sensors were fabricated using an established protocol with several slight modifications.[36,37,39] Specifically, before surface modification, the electrodes were manually polished on microcloth using 1 μm monocrystalline diamond solution and 0.05 μm alumina micropolish powder for 1−2 min each. Electrodes were sonicated for 5 min after each polishing step to remove excess polishing particles. After mechanical polishing, the electrodes were subjected to several electrochemical cleaning steps by cycling the potential (−0.35 to 1.5 V vs Ag/AgCl and ν = 100 mV/s) in a 0.05 M H$_2$SO$_4$ solution until a reproducible voltammogram was achieved. The cleaned electrodes were then subjected to stepwise self-assembled monolayer formation to create the E-AB sensor surface. The electrodes were modified with a layer of thiolated aptamer probes by immersing the electrodes into desired buffer solutions with aptamer concentrations of 1 μM for 8 h or overnight (~16 h) at room temperature for ATP or tobramycin sensors, respectively. This step was followed by immersing the electrodes into a 30 mM mercaptohexanol solution overnight (~16 h) or 5 h to form a self-assembled monolayer (SAM) of mercaptohexanol to passivate the remaining electrode surface.[46] These sensor fabrication conditions were determined vide infra to be optimal for the respective sensor performance. For the nanostructured electrodes, prior to sensor modification, clean electrodes were immersed in a stirred solution of 1.2 mg/mL HAuCl$_4$, 0.1 M NaCl, and 1.5 wt % HCl. A pulsed waveform from 0.0 to −0.4 V (vs Ag/AgCl) with a frequency of 1 Hz for 60 s is applied to reduce and deposit gold onto the electrode surface.[23,24,26,47] Finally, all sensors were interrogated using squarewave voltammetry with a frequency of 60 Hz, a pulse amplitude of 25 mV, and a voltage increment of 1 mV.

RESULTS AND DISCUSSION

Combining the positive attributes of microelectrodes with the specific recognition capabilities of aptamer-based sensors represents a promising bioanalytical sensing platform with improved spatiotemporal resolution over traditional macroscale sensors. In this report, we employ two representative faradaic folding-based E-AB sensors[29] on both control planar microelectrodes (smooth surfaces) and nanostructured microelectrodes. The signaling mechanism of the sensors relies on a target-

induced conformation or flexibility change in the redox-labeled aptamer. This change alters the efficiency with which the redox marker transfers electrons with the interrogating electrode thus changing the faradaic current measured (Scheme 1).[29,33] Salamifar and Lai recently reported a similar detection methodology using E-DNA (or electrochemical, DNA-based sensors) on nanometer-scale electrodes for the detection of complementary DNA sequences. The electrodes are fabricated by depositing dendritic gold nanostructures onto recessed platinum nanopore electrodes.[26] The novel data presented by Salamifar and Lai is qualitative, demonstrating signal change in the presence of complementary DNA target strands. A common strength of folding-based E-DNA and E-AB sensors is their ability to be regenerated as a result of their reagentless nature.[33] In the report by Salamifar and Lai, however, sensor regeneration is problematic. In this report, for the first time, we report on the successful development of reproducible and quantitative folding-based E-AB sensors on small-scale electrodes. We present a comprehensive study of the challenges and successes in developing these sensors.

Planar Microelectrode-Based Sensors and the Consequence of Oxygen Reduction. Initial attempts at fabricating E-AB sensors on 25-μm-diameter planar microelectrodes were not successful. The sensors failed as a result of both unstable square wave voltammetric peak currents and large background currents. Specifically, the observed peak current resulting from the reversible reduction of the tethered methylene blue was typically small, on the order of several picoAmps or lower, which was not discernible above background currents (Figure 1). While state-of-the-art potentiostats

Figure 1. Background current resulting from the reduction of dissolved oxygen overwhelms any observable current from the reversible reduction of the tethered methylene blue. Planar microelectrode, electrochemical, aptamer-based sensors exhibit large oxygen reduction peaks (black) when employed directly in buffer solution. This peak interferes with the methylene blue reduction peak. Deoxygenating the solution by purging with nitrogen removes the oxygen reduction peak to yield small yet observable methylene blue reduction peak (blue line and inset).

are capable of measuring such currents, the problem is exacerbated by the appearance of a large background current presumably a result of the irreversible reduction of dissolved oxygen (Figure 1). Sensors run in buffer without a deoxygenation step typically exhibit a wide square wave voltammetric peak centered at ~−0.34 V (vs Ag/AgCl—although the peak potential often shifts). Similar oxygen reduction peaks were observed at mercaptohexanol modified

electrode surfaces by Creager and Olsen.[48] After a deoxygenation procedure by purging buffer with nitrogen for 30 min, this peak was eliminated (Figure 1). In turn, a small-magnitude reduction peak is observed at ~−0.25 V (vs Ag/AgCl) corresponding to the reduction of methylene blue (Figure 1).

Unfortunately, the majority of the sensors fabricated on planar microelectrodes exhibit square wave voltammograms overwhelmed by the observance of an oxygen reduction peak thus precluding any reproducible quantitative measurements based on the faradaic signal from methylene blue. Of note, we were able to observe qualitative changes in the oxygen reduction peak current as a function of target ATP addition (Figure 2). Sensors were fabricated with an 1 h incubation in
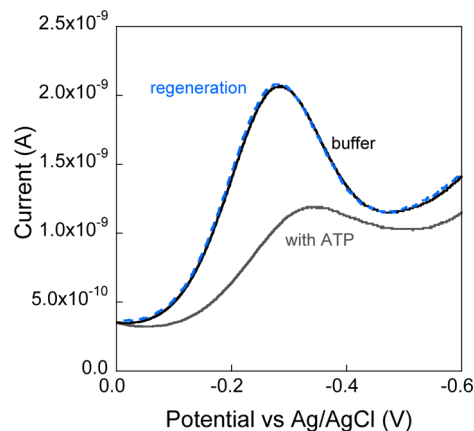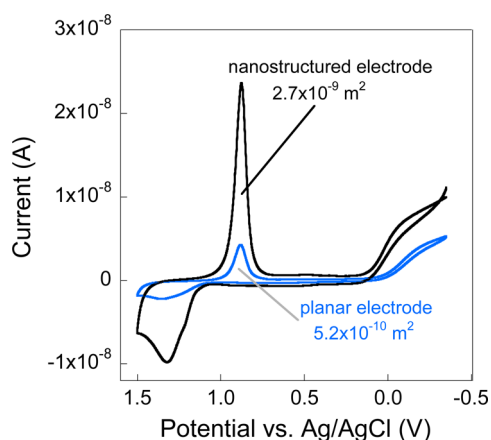

Figure 2. Changes in the current magnitude related to oxygen reduction can potentially provide a sensing transduction mechanism for folding-based E-AB sensors. Specifically, ATP sensors fabricated on planar gold microelectrodes exhibit large oxygen reduction currents that change in a signal off manner to the presence of ATP. The presumed mechanism follows an impedance-like sensing mechanism in which the conformation change alters the accessibility of oxygen reaching the surface to generate faradaic current. Unfortunately, sensor-to-sensor variability is too large thus precluding further measurements and is the subject of current investigations.

100 nM ATP aptamer followed by a 1 h modification in 3 mM mercaptohexanol. The sensors respond to the addition of ATP in a signal-off manner and can be regenerated (Figure 2). This signaling polarity is opposite from what is expected for this aptamer-based sensor.[38] The proposed mechanism is that the conformation change in the aptamer affects the accessibility of oxygen diffusing to the electrode surface and thus creates a change in observable current similar to impedimetric-based sensors employing redox markers.[49−51] The folded aptamer further blocks accessibility to the surface thus resulting in a decrease in current. The sensor signal response based on oxygen reduction, however, varies widely from sensor to sensor in terms of both magnitude and peak potential (as seen in Figures 1 and 2) and was difficult to reproduce. This phenomenon is currently under investigation by our laboratory, however we did not pursue this as a viable method for target quantification in this manuscript.

The presence of the oxygen reduction peak indicates that the passivating monolayer is poorly packed leaving many defect sites, or accessible sites for oxygen to be reduced.[48,52,53] This poor packing reveals many surface sites that, on average, likely represent a larger percentage of the overall surface area in contrast to sensing monolayers formed on large-scale electrodes

(on which E-AB sensors function reproducibly).[30,31,35−38,40] While several attempts were made to improve the quality of the passivating monolayer through higher thiol concentration and/ or longer deposition times, we were unable to consistently achieve low background signals. In addition, a more robust passivating monolayer (e.g., longer chain alkanethiols)[48,54,55] does not selectively reduce unwanted background currents and thus signal from methylene blue reduction was also impeded.

Microelectrodes with a Nanostructured Surface are Suitable for E-AB Sensor Fabrication. To circumvent the complication of small sensor currents, we increased the electroactive surface area of the interrogating microelectrode via the electrodeposition of dendritic gold structures.[24,25,47] Specifically, potentiostatic deposition of dendritic gold structures using a gold chloride solution, previously described by Lai and co-workers,[47] yields gold electrode surfaces with significantly larger surface area (Figure 3 and S1 in Supporting Information). The deposition is achieved by the reduction of gold onto the microelectrode surface while applying a pulsed potential between 0.0 and −0.4 V (vs Ag/AgCl) in a stirred gold chloride solution. The amount of gold and the nature of the morphology is a function of the amount of time this potential pulse is applied and the frequency of the application (pulsed or constant, see Supporting Information Figure S1). We determined vide infra that deposition of gold structures using a pulsed waveform from 0.0 to −0.4 V with a frequency of 1 Hz for 60 s yields the most reproducible sensor surface out of the conditions studied. This pulsed surface preparation protocol is used for all later described experiments unless otherwise noted. Electrochemical characterization of the gold nanostructured surfaces demonstrates consistent and reproducible increases in the electroactive surface area. Specifically, we use the gold oxide reduction peak obtained via cyclic voltammetry in a 0.05 M H_2SO_4 to quantify the surface area of the resulting electrode (Figure 3). Integration of the reduction peak area allows calculation of the electrode surface area using a literature reported value for the reduction of a gold oxide layer (400 $\mu C/cm^2$).[56] Our optimal deposition waveform yields a $6._1 \pm 1._6$-fold increase in electroactive surface area.

Microelectrodes with the deposited gold nanostructures supports improved sensor performance. E-AB sensors for the


Figure 3. Electrodeposition of dendritic nanostructures increases the electroactive surface area of the gold microelectrode. Comparison of the gold oxide reduction peaks in 0.05 M H_2SO_4 before (blue) and after (black) deposition reveal an on average $6._1 \pm 1._6$-fold increase in electroactive surface area.

detection of ATP fabricated on the nanostructured electrode surfaces exhibit significantly larger currents associated with methylene blue reduction (Figures 4 and 5). Typical methylene
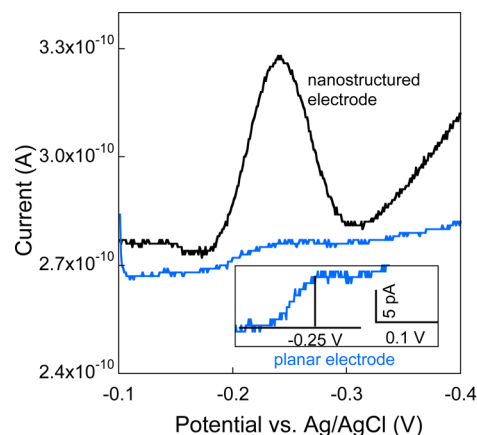

Figure 4. Nanostructured gold microelectrodes are suitable for the fabrication of E-AB sensors. ATP sensors fabricated on nanostructured microelectrodes exhibit increased current signal resulting from the reduction of methylene blue reduction (black line) in comparison to the planar (blue line and inset) 25 μm gold electrodes.

blue peak currents range from ∼50 pA to several hundred pA which is likely a result of both the increased surface area of the electrode as well as differences in the packing density and reduced steric hindrance between neighboring probes because of the nanostructured surface. Furthermore, while there is the foot of an oxygen reduction peak at more negative potentials (<∼−0.35 V vs Ag/AgCl) when the sensor is challenged in tris buffer, the methylene blue signal is large in comparison. Still, with this improved signaling, the stability of the sensor surface in tris buffer remained an issue (Figure 5 and Supporting Information Figure S2). Over time and successive voltammetric scans, we continued to observe an increase in the oxygen reduction peak (Figure 5, left). This observation points again to the fact that the integrity of the self-assembled monolayer remains a limiting issue.[57]

Blood Serum Suppresses Oxygen Reduction Current. Sensors fabricated on the nanostructured microelectrodes exhibit more stable current and performance when employed directly in 100% undiluted serum. Specifically, when the ATP E-AB sensors were employed directly in serum we observe reproducible suppression of the current resulting from oxygen reduction (Figure 5 right). After a 120 min equilibration period in serum, during which the methylene blue reduction peak magnitude also reduces (up to ≤∼40%) to a stable value (presumably from nonspecific adsorption of serum proteins), the baseline currents are more stable and free of background signal from dissolved oxygen (Figure 5 right). We discuss this observation in detail below.

Employment of micro-E-AB sensors for the quantification of ATP directly in 100% undiluted serum enabled reproducible, stable, and quantitative sensor measurements (Figure 6). The sensors were prepared as described above and after preparation, sensors were incubated in serum for ∼120 min. Upon addition of ATP to the serum, the methylene blue peak current increased as expected (Figure 6, left and middle). This increase in signal occurred monotonically with ATP concentrations and was fit to a Langmuir-type binding isotherm by plotting the percent signal change (percent signal change = $((i_{[ATP]} - i_0)/i_0)$
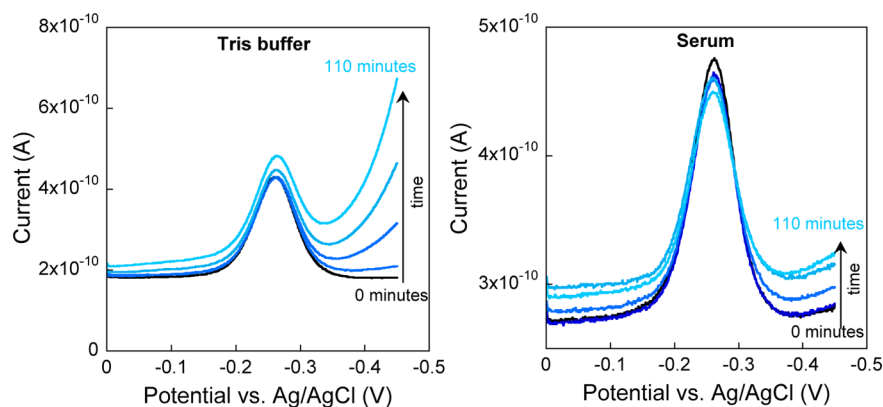
Figure 5. Employment of E-AB sensors for ATP detection directly in 100% undiluted blood serum provides suppression of observable oxygen reduction current. (Left) The background current results from the reduction of dissolved oxygen in tris buffer increases over time and distorts signal results from tethered methylene blue reduction. (Right) Conversely, sensors challenged in undiluted serum maintain a stable background current with suppressed current signal from the reduction of oxygen.
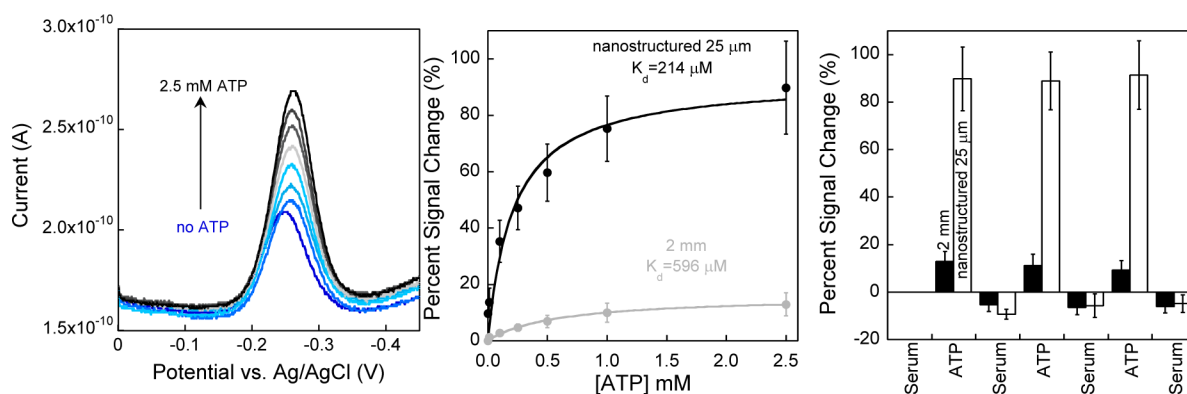

Figure 6. Electrochemical aptamer-based ATP sensors based on microelectrodes with dendritic nanostructures demonstrate enhanced and reproducible performance in 100% bovine serum. (Left) Addition of ATP analyte results in a quantitative increase in faradaic peak current from the reduction of methylene blue. (Middle) The nanostructured 25 μm sensors demonstrate an enhanced binding affinity and signal change in comparison to sensors fabricated on 2 mm diameter electrodes using the same fabrication procedure. (Right) Finally, these nanostructured 25 μm sensors demonstrate reproducible performance. Signal can be regenerated by rinsing with serum containing no ATP. All data represents the average and standard deviation of at least three independent sensors.
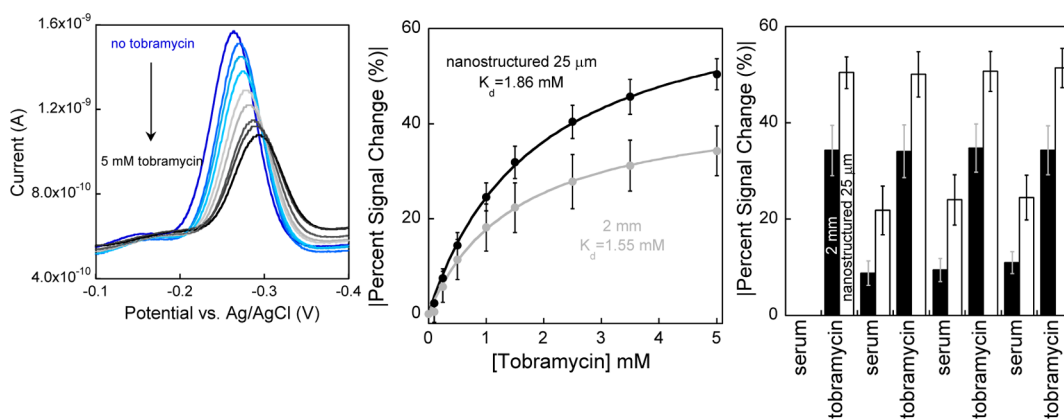
Figure 7. Stable performance of nanostructured microelectrode E-AB sensors in 100% serum is a general trend. (Left and middle) Electrochemical aptamer-based sensors for the detection of the aminoglycoside antibiotic exhibits quantitatively decreased current signal to the presence of tobramycin. (Middle) The nanostructured sensors exhibit slightly improved sensitivity and similar binding affinity in comparison to sensors fabricated on 2 mm diameter gold electrodes using the same fabrication protocol (plotted as absolute value). (Right) Finally, the nanostructured 25 μm sensors demonstrate reproducible performance. Signal can be regenerated by rinsing with serum containing no tobramycin protocol (plotted as absolute value). All data represents the average and standard deviation of at least three independent sensors.

$\times$ 100%) as a function of ATP concentration (Figure 6, middle). From the binding isotherm, we calculated an observed

binding affinity of 214 μM and a maximum percent signal change of ~80%. As a point of comparison, we prepared

11421

dx.doi.org/10.1021/ac503407e | *Anal. Chem.* 2014, 86, 11417−11424
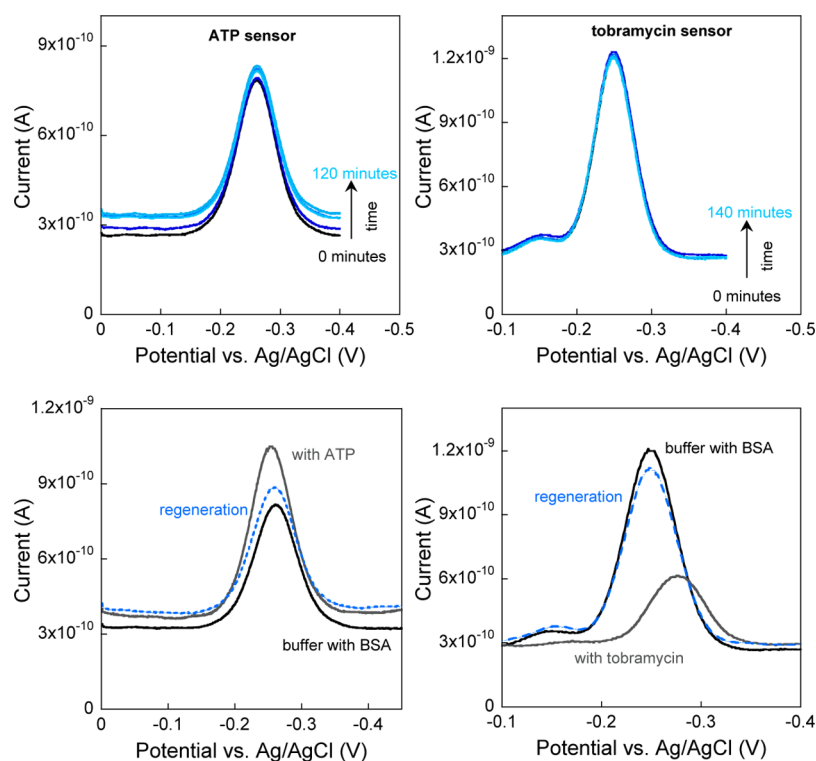
Figure 8. Nonspecific adsorption of BSA suppresses background currents from oxygen reduction and enables stable, reproducible sensor performance of microelectrode-based E-AB sensors. Specifically sensors fabricated to target (left) ATP and (right) tobramycin are stable over long time periods as indicated by the reproducible voltammograms. (Bottom left) The ATP sensor shows an increase in peak current with the addition of ATP and is able to be regenerated by immersion in BSA-containing buffer without ATP. (Bottom right) Likewise, the tobramycin sensor also exhibited regenerable signal with the presence and absence of tobramycin.

sensors on macroscale electrodes (2 mm diameter) using the same modification procedures. Interestingly, we find that the nanostructured microsensors exhibited significantly enhanced binding affinity and sensitivity (Figure 6, middle). Specifically, the macro sensor yielded an observed binding affinity of 596 μM and maximum signal change of ~20%. Finally, the nanostructured sensors also exhibited reproducible regeneration (Figure 6, right), demonstrating the reusability of the sensor. Throughout these experiments, which typically lasted ~8 h, we observed no degradation of the methylene blue signal or increase in signal from oxygen reduction.

To demonstrate the universality of our microsensor approach, we also developed sensors against aminoglycoside antibiotics using the DNA-based aptamer described by Rowe et al.[35] We observed the same challenges in developing microscale sensors for aminoglycosides as we observed with the ATP sensors—low and unstable current signals and large oxygen reduction background signals. Using the modification procedures described above, we fabricated microelectrode and macroelectrode sensors for the detection of the aminoglycoside antibiotic tobramycin. When employed directly in serum, the tobramycin sensor exhibited reproducible changes to the presence of tobramycin in a signal-off manner as expected (Figure 7 left and middle).[35] While the microscale sensor did exhibit a slightly better sensitivity than the macroscale sensors fabricated using the same conidtions, the difference between the micro- and macroscale sensors is less pronounced than what was observed with the ATP sensor. Nonetheless, the sensors are reproducible when employed in 100% serum (Figure 7 right). After a ~10% signal loss during the first regeneration, the sensor was regenerated to nearly 100% of the

original signal at each subsequent challenge and regeneration (typical performance of this class of sensor).[58]

The observance of improved sensor performance on nanostructured electrodes is not unprecedented. Several reports by Kelley and co-workers demonstrate that nanostructured surfaces enhance the capture ability of immobilized DNA and thus leads to improved sensitivities.[23−25] The hypothesis is that DNA immobilized onto nanostructured surfaces reduces steric hindrance from neighboring probes. This morphology thus allows higher accessibility of analyte to the nucleic acid, which leads to better observed-binding affinity and sensitivity. It is still unclear as to the origin of the difference in enhancement observed between our ATP sensor and the tobramycin sensor. While it is only speculative, the aptamer geometry and the nature of the conformation change may affect sensor behavior.

Non-Specific Adsorption of Proteins Passivates Defect Sites in the Sensing Monolayer. We hypothesized that the nonspecific adsorption of serum proteins acts to further passivate the electrode surface by filling in monolayer defect sites. To test our hypothesis, we fabricated sensors as discussed above for ATP and tobramycin on the nanostructured electrode surface. The sensors were incubated in a 30 mg/mL bovine serum albumin (BSA) in buffer solution for 2 h followed by sensor testing in the same solution to mimic tests in serum. BSA is the main protein found in bovine serum (~30 mg/mL)[59] and is widely used for biosensor surface passivation through nonspecific adsorption.[60−64] Both the ATP and tobramycin sensors exhibited more stable methylene blue-associated currents and reduced oxygen reduction backgrounds (Figure 8). Furthermore, the sensors exhibited reproducible performance responding and regenerating to challenges with

their respective targets (Figure 8). This evidence supports the hypothesis that the nonspecific adsorption of proteins to the surface of the electrode provides additional current suppression. We should note sensors fabricated with the same modification procedures that were incubated in a 30 mg/mL BSA in buffer solution for 2 h, followed by sensor tests in tris buffer without BSA exhibited unstable performance as indicated by an increase in the magnitude of the oxygen reduction peak over time (data not shown). This suggests that a continuous passivation is needed to protect the surface from further degradation of the passivating monolayer—a problem that does not appear to appreciably affect sensors on the macroscale. Once again, this passivation is not selective. We typically observe an <10% decrease in the methylene blue related signal after a 2 h incubation. This change is typically larger up to ~40% when the sensors are employed in serum. Nonetheless, this passivation sufficiently suppresses current associated with oxygen reduction and thus enables reproducible sensor performance.

CONCLUSION

In this report, we describe the challenges and successes of fabricating electrochemical, aptamer-based sensors using gold microelectrodes. We demonstrated, for the first time, the reproducible performance of folding-based E-AB sensors on microelectrodes using two representative small-molecule aptamer sensors. Critical to the stable performance of the resulting sensor is the integrity of the sensing self-assembled monolayer on the electrode surface. This monolayer provides both the recognition and signaling moiety (the redox labeled aptamer probe) and a passivating layer (mercaptohexanol).[46] Self-assembled monolayer chemistry enables the creation of a sensing surface that is specific for the target of interest while suppressing unwanted background currents nonfaradaic and faradaic alike. An observed consequence of a poorly formed monolayer is the emergence of a large faradaic background current resulting from the irreversible reduction of dissolved oxygen. While some attempts were made to quantitatively use this signal (see Figure 3), poor reproducibility precluded this as a viable signal transduction mechanism. Improvements in the passivating layer chemistries represent a challenge as well. While better passivation leads to more suppression of unwanted currents, it also suppresses the current associated with sensor signaling.

To facilitate the reproducible function of microelectrode-based E-AB sensors, we use a nanostructured electrode surface created by electrodeposition of dendritic-like gold structures, and we employ the sensors directly in 100% undiluted blood serum. The increase in surface area generates larger faradaic signal associated with the reduction of methylene blue for sensor measurements. The employment of the sensor in 100% blood serum results in the nonspecific adsorption of serum proteins to create an additional passivation layer to block unwanted background currents resulting from oxygen reduction.

Sensors built on small-scale electrodes (micro and nano) have the ability to provide analytical measurements with excellent spatiotemporal resolution and chemical specificity. Electrochemical, aptamer-based sensors represent a class of sensors that are rapid, reagentless, sensitive, and reusable with the ability to be applied to virtually any target analyte. Building E-AB sensors on microelectrodes thus has the potential to make significant impacts in the fields of chemical and biochemical analysis. The sensors developed here provide a

starting point for the development of reproducible E-AB sensors on small-scale electrodes.

ASSOCIATED CONTENT

Ⓢ Supporting Information

Scanning electron micrographs of the nanostructured surfaces and additional voltammograms showing oxygen reduction. This material is available free of charge via the Internet at http://pubs.acs.org.

AUTHOR INFORMATION

Corresponding Author
*E-mail: rjwhite@umbc.edu. Tel: 410-455-5053.

Present Addresses
[†]Samiullah Wagan: St. Louis University School of Medicine, St. Louis, MO 63103, United States.
[‡]Melissa Dávila Morris: National Cancer Institute, Bethesda, MD 20892, United States.
[§]James Taylor: Department of Chemistry, University of North Carolina, Chapel Hill, NC 27599, United States.

Notes
The authors declare no competing financial interest.

ACKNOWLEDGMENTS

REFERENCES

(1) Privett, B. J.; Shin, J. H.; Schoenfisch, M. H. *Anal. Chem.* **2010**, *82*, 4723−4741.
(2) Ronkainen, N. J.; Halsall, H. B.; Heineman, W. R. *Chem. Soc. Rev.* **2010**, *39*, 1747−1763.
(3) Bakker, E.; Pretsch, E. *Trends Anal. Chem.* **2008**, *27*, 612−618.
(4) Wang, J. *Chem. Rev.* **2008**, *108*, 814−825.
(5) Toghill, K. E.; Compton, R. G. *Int. J. Electrochem. Sci.* **2010**, *5*, 1246−1301.
(6) Suryanarayanan, V.; Wu, C. T.; Ho, K. C. *Electroanalysis* **2010**, *22*, 1795−1811.
(7) Bard, A. J.; Faulkner, L. R. *Electrochemical Methods: Fundamentals and Applications*, 2nd ed.; Wiley: New York, 1980.
(8) Zhang, B.; Galusha, J.; Shiozawa, P. G.; Wang, G. L.; Bergren, A. J.; Jones, R. M.; White, R. J.; Ervin, E. N.; Cauley, C. C.; White, H. S. *Anal. Chem.* **2007**, *79*, 4778−4787.
(9) Bard, A. J.; Fan, F. R. F.; Kwak, J.; Lev, O. *Anal. Chem.* **1989**, *61*, 132−138.
(10) Bard, A. J.; Mirkin, M. V. *Scanning Electrochemical Microscopy*, 2nd ed. ed.; CRC Press: Boca Raton, FL, 2012.
(11) Kuss, S.; Polcari, D.; Geissler, M.; Brassard, D.; Mauzeroll, J. *Proc. Nat. Acad. Sci.* **2013**, *110*, 9249−9254.
(12) Mezour, M. A.; Morin, M.; Mauzeroll, J. *Anal. Chem.* **2011**, *83*, 2378−2382.
(13) Kim, D.; Koseoglu, S.; Manning, B. M.; Meyer, A. F.; Haynes, C. L. *Anal. Chem.* **2011**, *83*, 7242−7249.
(14) Zhang, B.; Adams, K. L.; Luber, S. J.; Eves, D. J.; Heien, M. L.; Ewing, A. G. *Anal. Chem.* **2008**, *80*, 1394−1400.
(15) Trouillon, R. l.; Ewing, A. G. *ACS Chem. Biol.* **2014**, *9*, 812−820.
(16) Xiao, N.; Venton, B. J. *Anal. Chem.* **2012**, *84*, 7816−7822.
(17) Ross, A. E.; Venton, B. J. *Anal. Chem.* **2014**, *86*, 7486−7493.
(18) Park, J.; Aragona, B. J.; Kile, B. M.; Carelli, R. M.; Wightman, R. M. *Neuroscience* **2010**, *169*, 132−142.

(19) Polcari, D.; Kwan, A.; Van Horn, M. R.; Danis, L.; Pollegioni, L.; Ruthazer, E. S.; Mauzeroll, J. *Anal. Chem.* **2014**, *86*, 3501−3507.

(20) Lugo-Morales, L. Z.; Loziuk, P. L.; Corder, A. K.; Toups, J. V.; Roberts, J. G.; McCaffrey, K. A.; Sombers, L. A. *Anal. Chem.* **2013**, *85*, 8780−8786.

(21) Llaudet, E.; Hatz, S.; Droniou, M.; Dale, N. *Anal. Chem.* **2005**, *77*, 3267−3273.

(22) Liu, G.; Sun, C.; Li, D.; Song, S.; Mao, B.; Fan, C.; Tian, Z. *Adv. Mater.* **2010**, *22*, 2148−2150.

(23) Bin, X. M.; Sargent, E. H.; Kelley, S. O. *Anal. Chem.* **2010**, *82*, 5928−5931.

(24) Das, J.; Kelley, S. O. *Anal. Chem.* **2013**, *85*, 7333−7338.

(25) Soleymani, L.; Fang, Z. C.; Sargent, E. H.; Kelley, S. O. *Nat. Nanotechnol.* **2009**, *4*, 844−848.

(26) Salamifar, S. E.; Lai, R. Y. *Anal. Chem.* **2014**, *86*, 2849−2852.

(27) Tuerk, C.; Gold, L. *Science* **1990**, *249*, 505−510.

(28) Ellington, A. D.; Szostak, J. W. *Nature* **1990**, *346*, 818.

(29) Liu, J.; Morris, M. D.; Macazo, F. C.; Schoukroun-Barnes, L. R.; White, R. J. *J. Electrochem. Soc.* **2014**, *161*, H301−H313.

(30) Radi, A.-E.; Acero Sánchez, J. L.; Baldrich, E.; O'Sullivan, C. K. *J. Am. Chem. Soc.* **2006**, *128*, 117−124.

(31) Baker, B. R.; Lai, R. Y.; Wood, M. S.; Doctor, E. H.; Heeger, A. J.; Plaxco, K. W. *J. Am. Chem. Soc.* **2006**, *128*, 3138−3139.

(32) Liu, Y.; Yan, J.; Howland, M. C.; Kwa, T.; Revzin, A. *Anal. Chem.* **2011**, *83*, 8286−8292.

(33) Lubin, A. A.; Plaxco, K. W. *Acc. Chem. Res.* **2010**, *43*, 496−505.

(34) White, R. J.; Plaxco, K. W. *Anal. Chem.* **2009**, *82*, 73−76.

(35) Rowe, A. A.; Miller, E. A.; Plaxco, K. W. *Anal. Chem.* **2010**, *82*, 7090−7095.

(36) Schoukroun-Barnes, L. R.; Wagan, S.; White, R. J. *Anal. Chem.* **2013**, *86*, 1131−1137.

(37) White, R. J.; Phares, N.; Lubin, A. A.; Xiao, Y.; Plaxco, K. W. *Langmuir* **2008**, *24*, 10513−10518.

(38) White, R. J.; Rowe, A. A.; Plaxco, K. W. *Analyst* **2010**, *135*, 589−594.

(39) Xiao, Y.; Lai, R. Y.; Plaxco, K. W. *Nat. Protoc.* **2007**, *2*, 2875−2880.

(40) Xiao, Y.; Lubin, A. A.; Heeger, A. J.; Plaxco, K. W. *Angew. Chem., Int. Ed.* **2005**, *44*, 5456−5459.

(41) Huizenga, D. E.; Szostak, J. W. *Biochemistry* **1995**, *34*, 656−665.

(42) Wang, Y.; Rando, R. R. *Chem. Biol.* **1995**, *2*, 281−290.

(43) Wang, G. L.; Zhang, B.; Wayment, J. R.; Harris, J. M.; White, H. S. *J. Am. Chem. Soc.* **2006**, *128*, 7679−7686.

(44) Liu, J.; Kvetny, M.; Feng, J. Y.; Wang, D. C.; Wu, B. H.; Brown, W.; Wang, G. L. *Langmuir* **2012**, *28*, 1588−1595.

(45) Liu, J.; Wang, D. C.; Kvetny, M.; Brown, W.; Li, Y.; Wang, G. L. *Langmuir* **2013**, *29*, 8743−8752.

(46) Herne, T. M.; Tarlov, M. J. *J. Am. Chem. Soc.* **1997**, *119*, 8916−8920.

(47) Yang, W. W.; Gerasimov, J. Y.; Lai, R. Y. *Chem. Commun.* **2009**, 2902−2904.

(48) Creager, S. E.; Olsen, K. G. *Anal. Chim. Acta* **1995**, *307*, 277−289.

(49) Liu, G.; Sun, C. F.; Li, D.; Song, S. P.; Mao, B. W.; Fan, C. H.; Tian, Z. Q. *Adv. Mater.* **2010**, *22*, 2148−2150.

(50) Li, X. X.; Shen, L. H.; Zhang, D. D.; Qi, H. L.; Gao, Q.; Ma, F.; Zhang, C. X. *Biosens. Bioelectron.* **2008**, *23*, 1624−1630.

(51) Kafka, J.; Panke, O.; Abendroth, B.; Lisdat, F. *Electrochim. Acta* **2008**, *53*, 7467−7474.

(52) Wink, T.; J. van Zuilen, S.; Bult, A.; P. van Bennekom, W. *Analyst* **1997**, *122*, 43R−50R.

(53) Guo, L.-H.; Facci, J. S.; McLendon, G.; Mosher, R. *Langmuir* **1994**, *10*, 4588−4593.

(54) Lai, R. Y.; Seferos, D. S.; Heeger, A. J.; Bazan, G. C.; Plaxco, K. W. *Langmuir* **2006**, *22*, 10796−10800.

(55) Ricci, F.; Zari, N.; Caprio, F.; Recine, S.; Amine, A.; Moscone, D.; Palleschi, G.; Plaxco, K. W. *Bioelectrochemistry* **2009**, *76*, 208−213.

(56) Angerstein-Kozlowska, H.; Conway, B. E.; Hamelin, A.; Stoicoviciu, L. *J. Electroanal. Chem.* **1987**, *228*, 429.

(57) Creager, S. E.; Olsen, K. G. *Anal. Chim. Acta* **1995**, *307*, 277−289.

(58) Kang, D.; Zuo, X.; Yang, R.; Xia, F.; Plaxco, K. W.; White, R. J. *Anal. Chem.* **2009**, *81*, 9109−9113.

(59) Boitano, A.; Ellman, J. A.; Glick, G. D.; Opipari, A. W. *Canc. Res.* **2003**, *63*, 6870−6876.

(60) Jeyachandran, Y.; Mielczarski, J.; Mielczarski, E.; Rai, B. *J. Colloid Interface Sci.* **2010**, *341*, 136−142.

(61) Lai, S.; Wang, S.; Luo, J.; Lee, L. J.; Yang, S.-T.; Madou, M. J. *Anal. Chem.* **2004**, *76*, 1832−1837.

(62) Steinitz, M. *Anal. Biochem.* **2000**, *282*, 232−238.

(63) Taylor, S.; Smith, S.; Windle, B.; Guiseppi-Elie, A. *Nucl. Ac. Res.* **2003**, *31*, e87−e87.

(64) Zhang, Z.; Zhang, M.; Chen, S.; Horbett, T. A.; Ratner, B. D.; Jiang, S. *Biomaterials* **2008**, *29*, 4285−4291.